# Air Pulsed-Corona discharges for degradation of emerging pharmaceutical pollutants in water and toxicity by-products control

Djakaou Iya-Sou, Nofel Merbahi, Jalloul Bouajila, Mohammed Yousfi

Journal of Water Process Engineering 67 (2024) 106127

Contents lists available at ScienceDirect

Journal of Water Process Engineering

journal homepage: www.elsevier.com/locate/jwpe

# Air Pulsed-Corona discharges for degradation of emerging pharmaceutical pollutants in water and toxicity by-products control

Djakaou Iya-Sou [a,b,*], Nofel Merbahi [a,*], Jalloul Bouajila [c], Mohammed Yousfi [a]

[a] Laboratoire Plasma et Conversion d'Energie (LAPLACE), Université Toulouse, UMR CNRS 5213, 31062 Toulouse, France
[b] Department of Chemical Engineering, School of Chemical Engineering and Mineral Industries, University of Ngaoundéré/Cameroon, BP 454 Ngaoundéré, Cameroon
[c] Laboratoire de Génie Chimique, Université de Toulouse, CNRS, INP, UPS, F-31062 Toulouse, France

ARTICLE INFO

Editor: Jing Zhang

*Keywords:*
Corona Discharge Patterns
Pharmaceuticals pollutants
Paracetamol
By-products
Toxicity control

ABSTRACT

The present study, based a tip-to-plane pulsed corona setup, examined the effects of tip-water distance, radius of curvature of electrode tip, and pulse voltage on the production of liquid-phase RONS used an indicator of degradation performance. Measurements of long-lived RONS species (nitrates, nitrites and $H_2O_2$) in deionized water were specifically analyzed. The optimum conditions were used for the removal of a high concentration (500 mg/L) of 4-acetaminophen (i.e. paracetamol) with study of oxidation by-products and their toxicity. The results showed that optimum RONS production in the liquid phase occurred for a short gap distance (4 mm), a tip curvature radius of 100 μm and a pulsed voltage of 10 kV and 10 kHz corresponding to an energetic corona spark regime which is characterized by optical emission spectroscopic measurements. Using these optimal corona discharge parameters, the study showed that after 30 min of exposure to the air plasma, 60 % removal efficiency was achieved at an initial paracetamol concentration of 500 mg/L based on HPLC-DAD sample analysis. GC–MS and LC-MS analysis of treated samples enabled us to identify and characterize two new by-products not previously identified in the literature: *N*-(4-(4-hydroxyphenylamino) phenyl) acetamide (*m/z*: 242) and *N*-(4-aminophenyl) acetamide (m/z: 150), most of which were nitrogen compounds. Further analysis of the toxicity of these by-products to the human cell line (HEK-293) demonstrated that the treated water was not toxic.

Overall, these results show that the CDP system is one of the best techniques for treating highly polluted wastewater.

## 1. Introduction

Pharmaceutical compounds have become an important category of water pollutants due to their increasing consumption in recent years [1,2] due to their ever-increasing quantities in natural water systems and groundwater. Nowadays, concentrations of pharmaceutical pollutants in the environment can reach huge amounts of parts per million (ppm). The presence of pollutants can be explained by the industrial expansion and the rapid growth of the human population, above all, by the secretion in urine and excrement of drugs not metabolized by humans or animals. Among these pollutants, non-steroidal anti-inflammatory drugs (NSAIDs) such as diclofenac (DCF), fluoxetine and paracetamol are common [3,4]. Acetaminophen (or paracetamol), a widely used and effective pharmaceutical analgesic worldwide, has been found in European surface waters and rivers [5]. The continuous release and infusion of paracetamol into aquatic environments and organisms can seriously harm the environment by causing genetic exchange and activating drug-resistant bacteria [5]. To disposal pharmaceutical pollutants such as paracetamol from aqueous solutions, various advanced oxidation processes (AOP), such as non-thermal plasma processes (NTP), have been considered [6,7].

Non-thermal or cold plasma processes have the advantage of producing a variety of highly reactive species, depending on the considered carrier gas. The reactive species are generated by cold plasma at atmospheric pressure, and especially those generated during plasma/liquid interactions. The interaction of NTP with water molecules produce some specific reactive species [8], such as $OH^{\cdot}$, $O^{\cdot}$, $H^{\cdot}$ $O_3$, $H_2O_2$, $NO^{\cdot}$, $^{\cdot}NO_2$…. In addition, **E**lectro**H**ydro**D**ynamic (EHD) movement of electrons at the interface may intensify the creation of new reactive molecules. The presence of water vapor due to evaporation phenomena in the gaseous plasma discharge zone can also promote the formation of new nitrogen and oxygen species such as peroxynitrite ($ONOO^-$), superoxide ($O_2^{\cdot-}$),

* Corresponding authors.
*E-mail addresses:* iya-sou@laplace.univ-tlse.fr (D. Iya-Sou), merbahi@laplace.univ-tlse.fr (N. Merbahi).

https://doi.org/10.1016/j.jwpe.2024.106127
Received 28 June 2024; Received in revised form 26 August 2024; Accepted 3 September 2024
Available online 10 September 2024

$HNO_3$, $HNO_2$ and others.

The controlled production of the oxidizing plasma species of interest can be considered in many fields as for instance the decontamination and sterilization of surfaces, the food preservation, the acceleration of seed germination and plant growth, the healing of chronic wounds, the functional group addition in dental field etc. [8].

To remove pollutant from wastewater, different varieties of electrical discharge plasma devices are presented in the literature [8,9] with a focus on optimizing formation and absorption of the RONS species of interest in the liquid phase, Liquid-plasma interactions generating aqueous RONS can be achieved by using either a powered electrode directly submerged in liquid thus creating a discharge in the liquid phase or by generating a plasma in the gas interface above the liquid surface.

We considered in this work the second setup using a powered electrode outside the liquid because the disadvantage of the use of submerged electrode is the higher energy consumption. In the considered plasma setup, the gaseous plasma reactive species impacting the liquid surface is affected by the direction of the electric field generating the plasma [10]. Furthermore, most plasma paracetamol degradation studies reported in the literature have focused on relatively low pollutant concentrations not exceeding 200 mg/L. For instance, for about 30 min of plasma exposure time, Korichi et al., [11]. reported that 68 % of paracetamol was eliminated from water using a plasma DBD setup while Slamani et al., reported 79 % of pollutant removal with an initial concentration of 200 mg/L [12]. Iervolino et al., reported 100 % elimination of paracetamol with an initial concentration of 25 mg/L [13]. Pan et al., reported 53.3 % elimination with an initial concentration of 100 mg/L [7]. Given the increasingly frequent detection of pharmaceutical pollutants in water, it is important to test the degradation efficiency of higher pollutant concentrations. Therefore, the main objective of the present work is to optimize a plasma device based on a positive pulsed corona setup for the treatment of higher concentrations of pharmaceutical pollutants (500 mg/L). As a model pollutant, we have chosen 4-acetaminophen (or paracetamol), a molecule difficult to degrade and abundant in the environment. In addition to paracetamol removal, particular attention has been paid to the formation and analysis of by-products after plasma treatment, and their toxicity will also be studied. In fact, this is generally an important aspect, as some by-products may be more toxic and carcinogenic than the original pollutant [14–16].

## 2. Experimental setups

### 2.1. Corona discharge setup

Fig. 1 shows the schematic diagram of corona discharge setup, which includes a tungsten tip with a curvature radius ranging from 20 to 100 μm. The tip can be moved along the Z axis using a micro-control device to adjust the inter-electrode distance (d) between the tip and the liquid surface. The high voltage mono-polar pulse was obtained by using an appropriate push-pull solid-state circuit high voltage pulse PVX 4110 at the output of a DC high-voltage generator (Technix HV SR10-R-300). This system can provide a high voltage pulse up to 10 kV, a frequency up to 10 kHz and a Pulse Width ranging from 500 ns to 100 ms. The volume of the exposed water was fixed at 100 mL contained in a Pyrex$^R$ crystallizer of 91 mm diameter, corresponding to a liquid height of 16 mm. A continuously operating magnetic stirrer homogenizes the spatial distribution of plasma species inside the liquid. The speed of rotation of the stirrer was regulated so as not to generate vortices in the liquid and to maintain a uniform tip-to-surface distance.

A metallic electrode was positioned at the bottom of the crystallizer and connected to the mass. The positioning of the mass favors the orientation of electric fields towards the plasma treated liquid, and positively influences the transport and diffusion of species from the gas phase to the liquid phase. The interface was regularly renewed by the magnetic stirrer.

The power supply delivers a high voltage mono-polar pulse, obtained by using an appropriate push-pull solid-state circuit high voltage pulse PVX 4110 at the output of a DC high-voltage generator (Technix HV SR10-R-300). This system can provide a high voltage pulse from 0 to 10 kV, a frequency up to 10 kHz and a Pulse Width range from 500 ns to 100 ms. The applied voltage (V) and instantaneous current i(t) are measured using a high voltage probe (Tektronix P6015A, with a maximum voltage rating of 40 kV pk PULSE) and a current monitor (Tektronix TCPA300), respectively, and simultaneously recorded using an oscilloscope (WaveSurfer 10, 1GHz and 10GS/s). The discharge

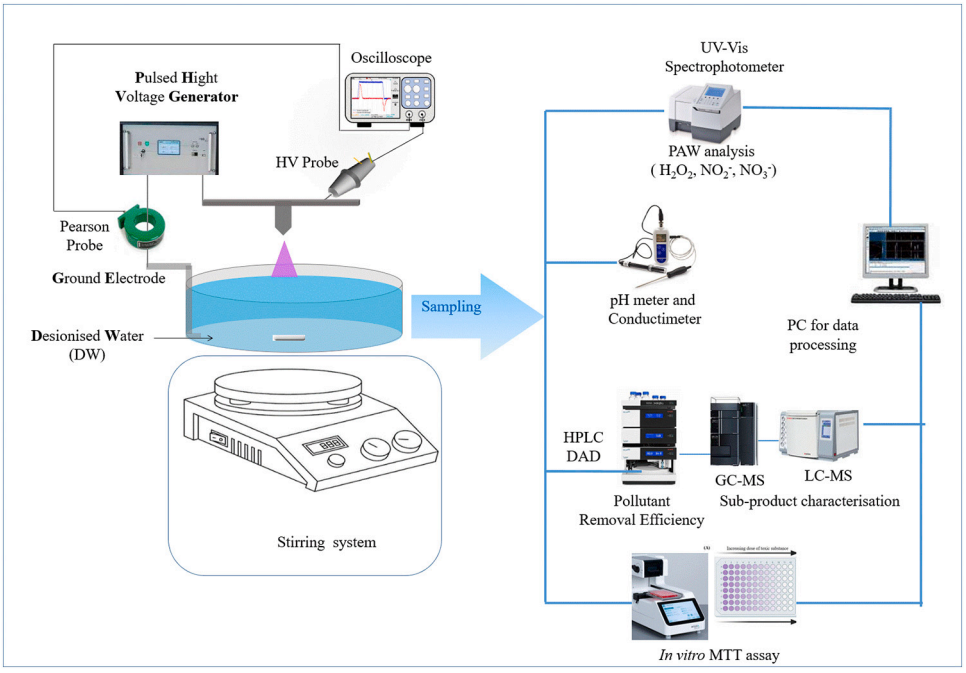


**Fig. 1. Left**: General view of the corona reactor (high-voltage tungsten carbide tip connected to its power supply and metal support, reaction medium, magnetic stirrer**). Right**: Measuring devices.

current was obtained by subtracting the displacement current (capacitive current), previously measured without discharge.

The operating parameters studied for this corona discharge setup can be classified into two types:

(i) Electrical parameters of power supply: applied voltage and pulse duration.

(ii) Geometric parameters: electrode gap (distance between tip and liquid surface).

As fixed parameters, we based our work on preliminary study carried out in the laboratory: 10 kHz as a frequency, pulse duration of 1000 ns and 100 μm as a radius of curvature. For this radius curvature value (100 μm), the branching structure of the plasma is more important at higher radius of curvature, which has a considerable influence on the conical shape of the discharge [17,18].

### 2.2. Optical emission spectroscopy

Optical emission spectroscopy is carried out using the Acton SP 2750 spectrometer (Teledyne Princeton Instruments, USA) with a focal wavelength of 0.75 m. With its three diffraction gratings, respectively 2400 tr/mm blazed at 250 nm, 1800 tr/mm at 500 nm and 600 tr/mm at 500 nm, a complete spectral scan from UV to infrared can be obtained. For this study, only the first two gratings were used to obtain an emission spectrum ranging from 200 to 800 nm. The photons emitted by the discharge are collected using a 600 μm diameter optical fiber connected to the spectrometer. To prevent second-order UV spectra from being superimposed on visible spectra, a filter preventing UV radiation from passing through is placed in front of the fibber. Acquisitions and processing are carried out using WinSpec32 processing software.

### 2.3. Materials and chemical reagents

In this study, paracetamol was chosen as the pharmaceutical model pollutant (chemical formula: $C_8H_9NO_2$, molecular weight: 151.163 g/mol, purity≥98 %, CAS number: 103–90-2). the initial concentration of paracetamol prepared in Deionized Water (DI) in our case is set at $[Pa]_0$ = 500 mg/L. Deionized water was used to avoid possible interferences due to the presence of molecules (ions) contained in ordinary water (tap water for example) and plasma, with the aim of better understanding the effect of plasma and the probable degradation mechanism of the pollutant used.

Detection and quantification of nitrates ($NO_3^-$), nitrites ($NO_2^-$) and hydrogen peroxide ($H_2O_2$) in demineralized water (DW) were carried out by multiphotometric analysis using a digital absorption spectrophotometer (UVline 9000C, Aqualabo, with associated reagents for specific analyses) equipped with light-emitting diodes (measurement wavelengths were 553, 530, 533 nm respectively) and a Si detector. pH and electrical conductivity measurements were carried out using a SevenGo Duo SG 25 multiparameter probe (Mettler Toledo).

The pollutant sample (paracetamol) was analyzed on high-performance analytical liquid chromatography (HPLC-DAD) using a C18 column (25 cm × 4.6 mm × 5 μm). The mobile phase composition used was 0.1 % (*v*/v) formic acid in laboratory-grade water (pH = 2.65) and acetonitrile solvent (80 %, pH = 2.65). The flow rate was maintained at 0.5 mL/min. Total analysis time was 30 min.

### 2.4. Gas Chromatography and Mass Spectrometry (GC–MS) Analysers

The Gas Chromatography Mass Spectrometry (GC–MS), Agilent 6890 gas chromatograph coupled to a 5975-mass detector enabled us to identify and analyze oxidation by-products in liquid phase. Analyses were carried out on non-derivatized and derivatized samples (addition of 60 μL of BSTFA (*N*, *O*-bis(trimethylsilyl)trifluoroacetamide) to the extracts (340 μL sample) and followed by a 30-min incubation at 40 °C), with a view to rendering compounds volatile. Batch experiments were performed at 25 °C [19].

### 2.5. UHPLC-MS, LC-MS

Samples analysis was performed using HPLC-MS. For this purpose, a Thermo Fisher UltiMate 3000 UHPLC (Sunnyvale, CA, USA) instrument connected to an Orbitrap high-resolution mass spectrometer (HRMS-Exactive, Waltham, MA, USA) was used. The electrospray ionization (ESI) source was programmed in the positive mode with a capillary, tube lens and skimmer voltage of 35.00 V, a capillary temperature of 300 °C and a spray voltage of 5.00 kV. The same C-18 column and gradient method as those used in the HPLC–DAD analyses were implemented. These parameters were selected and saved as direct infusion method for using Thermo Exactive (v. 1.1 Sp6) software of Thermo Exactive Orbitrap Mass spec. This method was integrated with HPLC method to create a single method for LCMS runs.

### 2.6. Cytotoxicity assessment: cell viability determination (MTT Test)

The toxicity of the by-products was evaluated on healthy HEK-293: embryonic renal epithelium cells by the MTT method "3-(4,5-dimethylthiazol-2-yl)-2,5-chdiphenyltetrazolium bromide (MTT) assessing cell viability assessment by evaluating mitochondrial function [20]. Relative values (%) of the total number of viable cells for each time point were calculated on the basis of the total number of HEK 293 cells in the sample-free control wells, used as 100 %. HEK-293 cells were distributed at 13 × $10^3$ cells/well in 96 microplates. After 24H incubation at 37 °C with 5 % $CO_2$, 100 μL of samples diluted in medium after being solubilized in DMSO were added to 100 μL of the corresponding appropriate culture medium. In our case, we used DMEM (Advanced DMEM, Thermo Fisher Scientific). The plate was then incubated for 48 h at 37 °C, and the cytotoxic potential of the test samples was assessed by the 3-(4, 5-dimethylthiazol-2-yl)-2,5-diphenyltetrazolium bromide (MTT) assay. After removal of the supernatant, the cells were treated with 50 μL of MTT solution. The plate was then incubated for 40 min at 37 °C, after which the MTT was removed and 80 μL of DMSO added. The absorbance was then read (Multiskan Go, F1–01620, Thermo Fisher Scientific, Vantaa, Finland) using a microplate reader at 605 nm to deduce the percentage viability of live cells. Tamoxifen at 37 mg/L concentration was used as a positive control.

### 2.7. Data analysis

Every set data in the present study had been replicated at three times of at least independent experiments. The reported data correspond to the mean ± standard.

## 3. Results and discussion

This section devoted to the results is divided into two parts:

i) Electric discharge parametric study in order to optimize the formation of some aqueous RONS species with a discussion on corona regime and its spectroscopic characterization.

ii) Treatment of paracetamol (as a pharmaceutical pollutant model) including the identification and the characterization of oxidation by-products and the cytotoxicity test on a healthy cell strain.

### 3.1. Effects of gap distance and applied voltage on RONS production and plasma spectroscopy

For this parametric study, the concentrations of specific stable species (Hydrogen Peroxide, Nitrites and Nitrates), pH and Conductivity (at 25 °C) of the liquid phase (deionized water) were chosen as indicators of optimal conditions. After some preliminary tests, we chose 2 constant parameters for this study to reduce the overall number of variables: plasma exposure time of liquid of 15 min, and a pulse duration of 1 μs.

*3.1.1. Effects of inter-electrode gap*

The effect of inter-electrode distance has been studied for a gap distance ranging from 4 to 10 mm while fixing voltage (6.5 kV) and frequency (10 kHz). The distances were chosen to ensure discharge stability and avoid arcing (for distances below 4 mm). The results displayed in Fig. 2 showed that increasing the gap distance induces a decrease of concentration of the stable species $H_2O_2$, $NO_2^-$, $NO_3^-$ and conductivity while the pH value significantly decreases. Optimal RONS concentrations in water are obtained for an inter-electrode distance of 4 mm.

For this gap of 4 mm, the concentrations of the species measured are 5 times higher than those obtained at an inter-electrode distance equal to 10 mm. For Nitrates, the inter-electrode distance has no effect from 8 mm upwards. The high concentration of nitrogen species obtained is the consequence of the pH decreases. This decrease can be explained by the following equations:

$$2NO_2 + H_2O \rightarrow HNO_3 + HNO_2 \quad (1)$$

$$O_3 + NO_2^- \rightarrow O_2 + NO_3^- \quad (2)$$

Conductivity is an indicator of the ionic charge in a medium [21]. The presence of RONS in the medium can strongly modifies conductivity [22,23]. In our case, when the inter-electrode spacing is low (4 mm), conductivity measured at 25 °C is two times greater than the 10 mm inter-electrode distance. The intensification of mass transfer coupled with species production in the liquid phase is strongly due to the integration surface between the gas and liquid phases, which are more intense for the smaller inter-electrode distance, as shown in Supplementary Data Fig. 1.

Supplementary Data Fig. 1 clearly shows the influence of the gap distance on the plasma generated and the gas/liquid interaction surface, when the distance between the electrode and the liquid surface increases, even if the voltage does not change, the discharge form, discharge current, and discharge power of the plasma will change. As can be seen from Supplementary Data Fig. 1, the larger the discharge distance, the smaller the contact area of plasma with the liquid surface, until there is no contact. This factor will greatly affect the produced species in the liquid. Thus, for 4 mm gap distance, the electrical effects of the discharge coupled with the spatial distribution of the electric discharge is larger and cover a larger plasma/liquid area as it can be seen in comparison to the 10 mm gap case. This intensifies at this interface the interactions between energetic electrons and both gaseous and liquid species. This therefore increases the density of primary species leading to RONS formation.

The choice of a pulsed power supply leads to the appearance of a

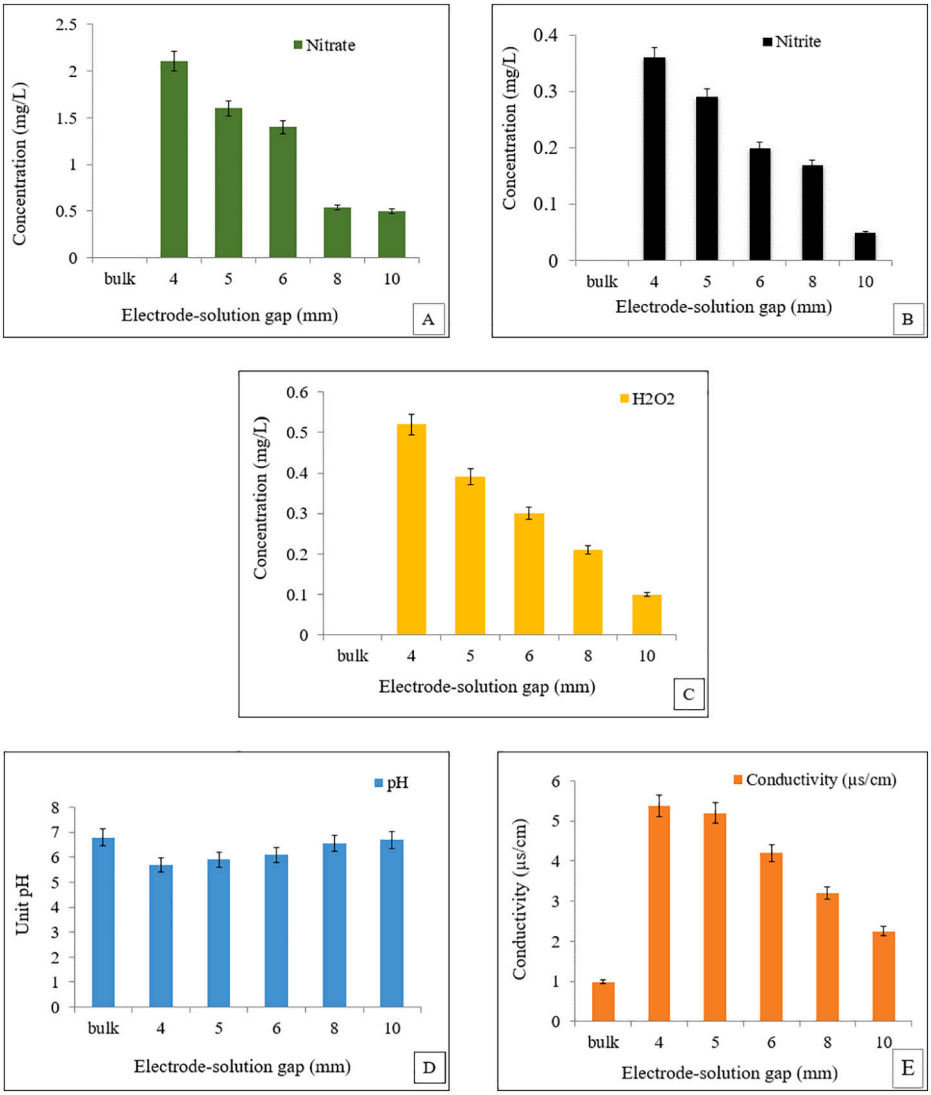


**Fig. 2.** (A, B, C) Concentrations of nitrates ($NO_3^-$), nitrites ($NO_2^-$) and hydrogen peroxide ($H_2O_2$), (D, E) Electrical conductivity (at 25 °C) and pH measured in deionized water after 15 min exposure to the Electrode-solution gap effect discharge (6.5 kV, 10 kHz, 1 µs, liquid volume of 100 mL, plasma exposure time 15 min).

multi-filament discharge (branching discharge structure), which has the advantage over the treatment of a liquid phase of generating more plasma species in the gas phase, but also of increasing the contact surface between the discharges, whose time-integrated profile has a conical appearance, and the liquid. The interaction diameter is of the order of 2–3 mm.

For the previous reasons, the distance between the tips and deionized water was set at 4 mm, in order to take full advantage of the larger spatial distribution of the electrical discharge that intensify the plasma interactions with the liquid surface.

### 3.1.2. *Effect of applied voltage*

Fig. 3 shows the influence of the applied voltage varying from 4.5 to 10 kV. For the set of used operating parameters, variations in the same quantities (RONS concentrations, conductivity, and pH) shows a drastic effect of voltage magnitude. $H_2O_2$ concentration rises from 0.11 mg/L for 4.5 kV to 110 mg/L for a voltage equal to 10 kV, while Nitrates vary from 0.91 mg/L (4.5 kV) to 150 mg/L (10 kV), Nitrite concentration from 0.13 to 4.6 mg/L, conductivity from 3.4 to 467 μs/cm and pH units decrease from 6 to 3.45.

The increase of RONS concentrations measured in the liquid phase can be explained by the transition from the streamer regime to the spark regime, whose characteristics are intermediate between streamer branching and arcing. The electrical characteristics of the streamer branching regime and spark regime, are measured for two input voltages of 4.5 kV to 10 kV respectively, as shown in Supplementary Data Fig. 2 and Supplementary Data Table.2. This shows that when switching from the streamer branching (4.5 kV) to spark regime (10 kV), the current increases by about a factor of 10, i.e., from 0.3 A to 3.5 A, and the power per pulse increases from 0.2 W for streamer branching regime (4.5 kV) to 95.27 W for spark regime at 10 kV.

In fact, in the spark regime compared to streamer the electrons have an energy higher and therefore more efficient to form the primary species precursor of RONS of our interest (see next subsection).

### 3.1.3. *Results on corona discharge regime and its spectroscopic characterization*

As already underlined, depending on the energy injected to ignite the

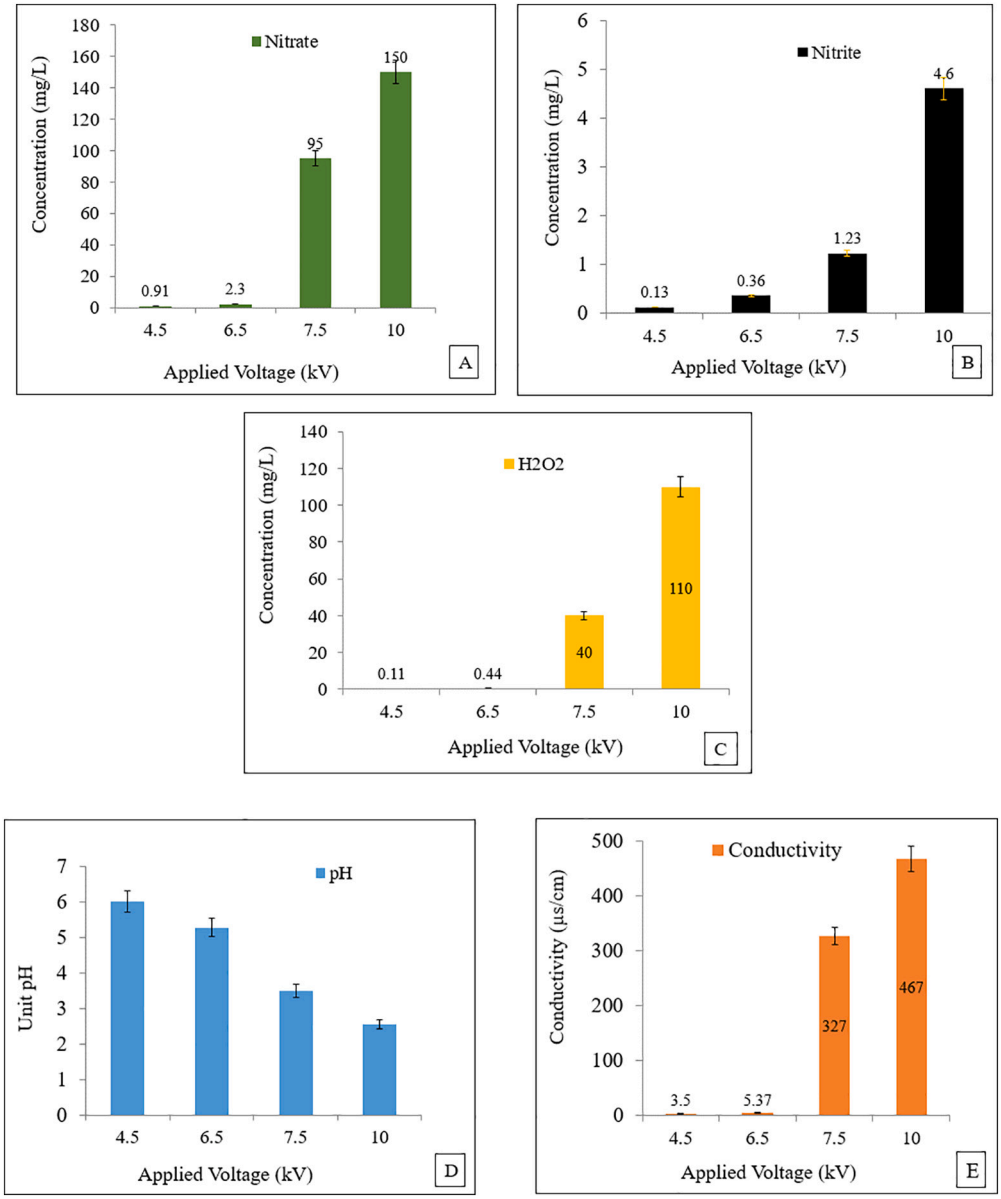


**Fig. 3.** (A, B, C) Concentrations of nitrates ($NO_3^-$), nitrites ($NO_2^-$) and hydrogen peroxide ($H_2O_2$), (D, E) Electrical conductivity (at 25 °C) and pH measured in deionized water after 15 min exposure to the power effect (10 kHz, 1 μs, 100 mL, 15 min, gap: 4 mm and 100 μm of tip radius).

electric discharge, the corona discharge regime evolves from a simple streamer at lower voltages (4.5 kV) to the spark mode obtained for higher voltages, as shown in Supplementary Data Fig. 3.

The streamer/spark transition takes place above 7.5 kV and induces a sharp increase of RONS plasma species densities in the liquid phase. The surface area interacting with the liquid phase is 10 times greater than in the streamer branching regime, of the order of 1 to 2 cm as shown in Fig. 4, will explain the formation and/or absorption in the liquid phase of much higher gaseous plasma species concentrations than in the case of the streamer branching regime.

It is known that spark mode causes local overheating of the gas by transferring high energy into the liquid phase compared to streamer mode. In spark mode, the liquid temperature rises from ambient temperature to 67 °C after only a few minutes of plasma-liquid contact. In contrast, in streamer branching mode, the liquid temperature is uniform and remains at ambient temperature throughout the treatment time. To explain this phenomenon of solution overheating, the rotational temperature of the gaseous plasma was estimated from spectroscopy together with the electron temperature Te and density N(e) [24,25].

First, for gas temperature, OH(A-X) spectrum is used since this is usually known as a good tool of rotational temperature ($T_{rot}$) estimation (see e.g., Ref [25]). And therefore of gas temperature ($T_{gas}$) because the relaxation times between rotation and translation state are very short. Therefore, $T_{gas}$ is estimated from OH(A-X) emission spectrum, emitted by the pulsed corona spark discharge in air in the range 306 and 310 nm. More generally, in the case of non-equilibrium electric discharges generated in humid gas for various electrode configurations, Trot can be obtained from the emission spectra between 306 nm to 310 nm corresponding to the transition OH(A-X) (i.e. $OH(A^2\sum,\upsilon = 0 \rightarrow X^2\prod,\upsilon' = 0)$). The fact that the non-equilibrium plasma is generated between a tip and a water surface tends to increase the concentration of gaseous OH species, resulting in clearer or more intense OH(A-X) spectra. This does not compromise the reliability of using the OH(A-X) spectrum as a thermometer for estimating Tgas as it is already underlined in the literature devoted to plasma liquid interactions (see e.g. ref. [8]).

In the present case, the OH(A-X) spectrum (Supplementary Data Fig. 3A), emitted by the pulsed spark in air, is situated on an emission continuum. Therefore, the red line base takes into account of such continuum due to bremsstrahlung associated to charged particles interactions and also a possible continuum due to chemiluminescence of nitrogen oxide.

The rotational temperature Trot equivalent to gas temperature is determined from comparison of experimental Branches Ratio $Q_2/0.5(R_1 + R_2)$ in our case to the calibration curve (Supplementary Data Fig. 4B) obtained from the synthetic spectra using LIFbase [25]. Further details on the methodology of $T_{rot}$ estimation can be found in ref. [24,25] $T_{rot}$ is therefore estimated to 3330 K with an error bar of about 400 K. This high temperature not representative of the plasma mean temperature since it corresponds to the highest temperature inside the spark structure, and it therefore clearly explains the exponential variation in liquid temperature when discharge is ignited in spark mode.

Furthermore, the electron temperature $T_e$ was then determined using the ratio Isps/Ifns of the intensities of the two close molecular nitrogen spectra of the second system positive $N_2$ SPS (2.5) and the first negative system $N_2^+$FNS (0.0) (see the zoom of Supplementary Data Fig. 5A) and also using the procedure described in detail in reference [24]. The obtained temperature $T_e$ is equal to 4.15 eV.

Last, the electron density $N_e$ was also determined from spectroscopy using the experimental broadening of the Hα line (Supplementary Data Fig. 5B). In fact, the starting point is the determination of apparatus broadening (close to 59 pm) for the considered spectrometer slit of 100 μm, the Doppler and collision broadenings (close to respectively 27 and 14 pm). Then from the knowledge of the full with of half maximum (FWHM) of the experimental Hα (FWHM = 187 pm), the Stark broadening was obtained by fitting the calculated Voigt spectrum and the experimental Hα line (FWHM Stark = 150 pm). Therefore, the estimated electron density $1.28 \times 10^{16}$ $cm^{-3}$ was directly deduced from the relation between electron density and Stark broadening given with the details on ($N(e^-)$) method of measurements in reference [24,25].

At this stage, it is important to emphasize that the electron density ($N(e^-)$) obtained for the spark regime (on the order of $10^{16}$) and the densities typically reported in the literature for the streamer regime (on the order of $10^{14}$) result in a density ratio between these two regimes of about 100. This ratio is roughly representative of the electric current ratio between the two regimes.

To have a precise idea on the main excited species generated in the chosen spark mode, Supplementary Data Fig. 6 (A and B) shows the emission spectrum in the UV and Visible range from 200 to 800 nm, for a grating equal to 2400 rpm, an acquisition time of 0.5 s and a gain of 100. The set of fixed parameters used are electrode voltage of 10 kV, pulse duration of 1 μs, inter-electrode gap of 4 mm, frequency of 10 kHz and 100 μm of tip radius.

As expected in discharge in ambient humid air, Supplementary Data Fig. 5A, shows a predominance of nitrogen species. The characteristic bands of Second Positive System (SPS) $N_2$ ($C^3\Pi_u$-$B^3\Pi_g$) between 323 and 415 nm with a central peak at 337.1 nm resulting from dissociation by electron impact (high electron densities in spark mode) on the $N_2$ molecule [26,27]. We also observe the characteristic NO band between

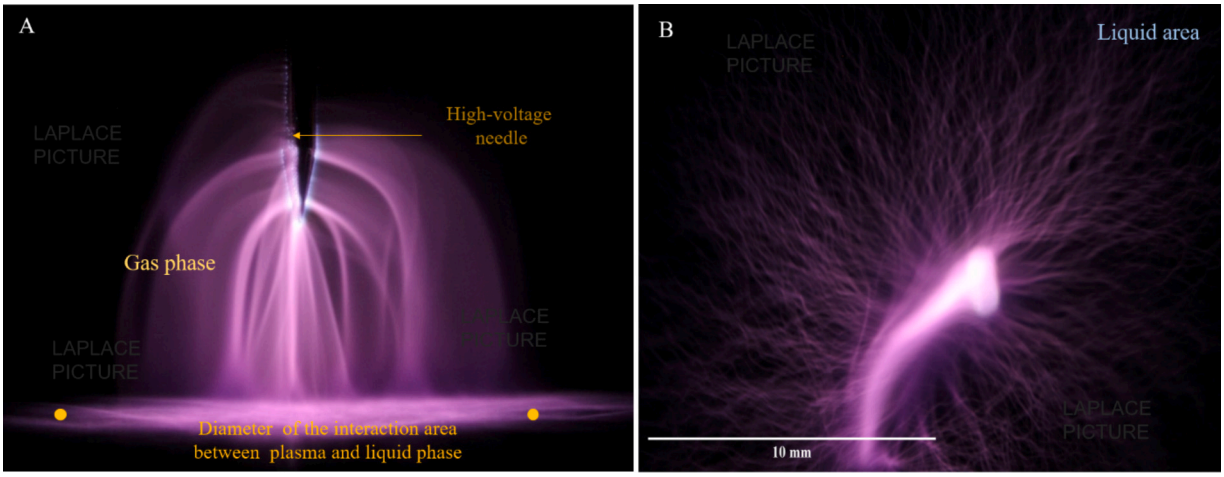


**Fig. 4.** (A) Demonstration of the conical shape of a corona discharge fed in pulsed mode and the increase in the surface area interacting with the liquid phase due to spark phenomena, (B) Instantaneous imagery capture showing the bottom view of the plasma contact surface with the liquid surface (10 kV, 10 kHz, gap: 4 mm, 1 μs, 100 mL and 100 μm of tip radius).

250 and 300 nm, which is the result of reaction between $N_2$ ($C^3\Pi_u$ -$B^3\Pi_g$) and oxygen [27]. The peaks obtained at 316, 337 and 357 nm are attributed to $N_2^*(C3\Pi u - B3\Pi g)$ [28]. The UV spectra (Supplementary Data Fig. 5A) we also observe a band at 309 nm attributed to OH(A-X) and reveals the presence of the First Negative System of $N_2^+$ (391 nm). In the visible range (400 to 800 nm, Supplementary Data Fig. 5B), we have $N_2$ bands at 415 nm, $H_\beta$ bands at 486 nm and a Gaussians band at 656 nm ($H_\alpha$). We also observed the oxygen triplet line at 777 nm [27].

The observed emission bands clearly show that the electronic impact, the energy, and the temperature-induced evaporation of the solution generated by the sparking regime considerably promote the formation of nitrogen and oxygen species in the plasma phase.

Finally, Table 1A summarizes the optimal electrical and geometrical parameters used for the present study of in situ paracetamol degradation while of the RONS species concentrations, pH and conductivity at 25 °C obtained for these optimal conditions are displayed in Supplementary Data Table 1. Overall, the electrons excite, dissociate and ionize the air molecules, generating high concentrations of primary species (·OH, O, N, etc.) all along each discharge filament from tip to water. These primary species when formed in the interface (by electron impact interactions or diffusion) interacts in turn with the surrounding air to form more stable secondary species following a chain of chemical reactions ($O_3$, $H_2O_2$, $ONOO^-$, $NO_3$, $NO_2$, etc.). The RONS of our interest are then formed in the liquid phase [8,28] from interactions of these primary and secondary species when interacting with the liquid surface.

In view of the results obtained for the spark mode, notably on the integration surface between plasma and liquid, and the reactive species measured in the liquid phase, the spark regime was chosen for paracetamol degradation. As a first step, it is necessary to carry out a spectral study to get a precise idea of the nature of some excited species formed in the gas phase.

### 3.2. Paracetamol removal by corona discharge patterns

This section is devoted to the analysis and discussion of the conversion rate of paracetamol, identification, and characterization of the subsequent by-products, including the possible paracetamol degradation pathways and the assessment of the in vitro cytotoxicity of these by-products. To study paracetamol degradation, experiments were carried out in spark mode for the reasons given in section 3.1 above (10 kV as applied voltage, 100 µm as tip radius, inter-electrode distance of 4 mm, 10 kHz as frequency, 100 mL as volume, and 1 µs as pulse duration).

#### 3.2.1. Paracetamol conversion rate

The performance of the spark discharge treatment was tested and evaluated for the degradation of paracetamol concentration of 500 mg/L over exposure time ranging from 0 to 30 min. Fig. 5 illustrates a noticeable increasing degradation of paracetamol versus the treatment time. For 30 min, the paracetamol degradation reaches 60 % with an energy efficiency value (G50) equal to 0.52 g/kWh as a performance indicator. The G50 value is chosen to minimize the interference effect of sub-product intermediate degradation, which may not be negligible at conversions above 50 %. However, it is difficult to perform an exhaustive comparison with other plasma configurations due to more particularly the initial concentration of the pollutant used in this work, i.e. 500 mg/L and also the differences on the considered plasma setups. But the result obtained in our case is particularly remarkable given the relatively high concentration of the dye (500 mg/L), which contrasts sharply with the findings of Korichi et al., and Iervolino et al., [11,13] using a non-thermal plasma (NTP) created by a dielectric barrier discharge (DBD) who reported respectively 60 % (4 g/kWh for G50) and 100 % (0.59 g/kWh) degradation but for an initial concentration of 25 mg/L, i.e. 20 times less. However, the efficiency yield (G50) obtained in our case are comparable to those obtained by Iervolino et al., despite the high concentration used (500 mg/L). To increase the efficiency of a plasma reactor, the mole ratio between the number of moles of reactive species and the number of moles of pollutant, ($\frac{n_{species}}{n_{paracetamol}}$) is an enhancement factor to consider.

Fig. 5 also shows that the degradation curve is not linear versus the treatment time, as confirmed by the linear transform ($\ln C_t/_{C0}$) derived from the degradation curve. This transform shows two phases: a very slow first phase between [0 and 15 min] and a second phase between [15 and 30 min]. Kinetic analysis of the linear transform shows two distinct degradation speeds that is associated to these two phases (Fig. 5).

Indeed, Fig. 5 shows that the degradation rate of phase 2 is 5 times higher than that of phase 1. The two phases obtained can be explained by the temperature regime of the solution, which would drastically influence the nature of the species produced in the plasma phase. As regards the temperature profile obtained, the temperature rises from room temperature to around 67 °C after 15 min and remains quasi-constant (67 °C) up to 30 min.

To dissociate the thermal effect and the plasma effect on the paracetamol degradation, an experiment was carried out respecting the temperature profile obtained throughout the degradation of the pollutant. No effect of temperature on pollutant degradation was observed. Pollutant degradation is therefore due to the primary and secondary species produced in the plasma phase and the associated physico-chemical processes who's the associated rate constants depend on temperature via the known Arhenius equation.

The two observed paracetamol degradation kinetics could be explained initially by the nature and flux of the species formed versus time, and by the competitiveness of reactivity between the paracetamol

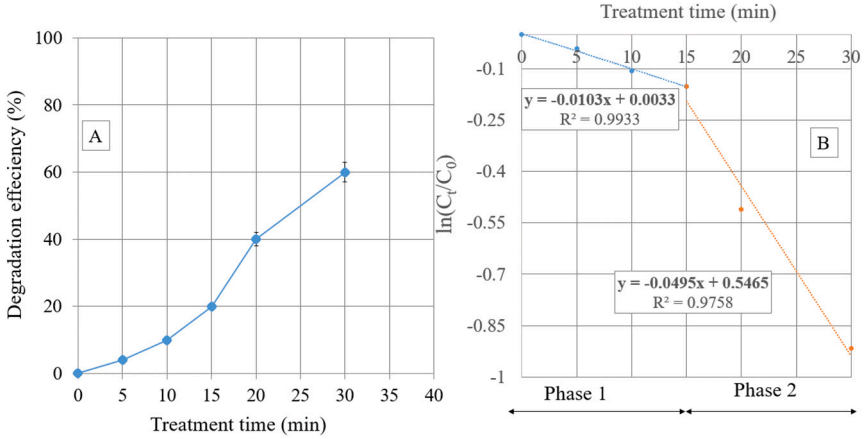


**Fig. 5.** (A) plasma effect on the degradation efficiency of paracetamol (500 mg/L) at different times (5, 10, 15, 20, 30 min), (B) kinetic degradation analysis storage time (10 kV, 10 kHz, gap: 4 mm,1 µs, 100 mL and 100 µm of tip radius).

molecule and the by-products formed versus exposure time. Several modelling studies of the production of species in the plasma phase have demonstrated the influence of temperature on their production: at low temperatures, there is a preference to produce oxygenated species (e.g., $O_3$) while at high temperatures, the production of nitrogenous species hindered because the dissociation threshold of oxygen is lower than the nitrogen one. In phase 2, the production of nitrogen oxides is therefore favored, which would explain the change in speeds obtained throughout the degradation process [29]. In fact, nitration of unsaturated compounds is faster than their oxidation [30,31]. The phenol molecule clearly illustrates this hypothesis. If we compare the reaction constants between phenol and ozone and its nitration by the $^{\cdot}NO_2$ radical, we have respectively $10^6$ L*mol$^{-1}$ s$^{-1}$ and $10^{10}$ L*mol$^{-1}$ s$^{-1}$, i.e. a factor of $10^4$. Added to this difference is the low absorption of oxygenated species compared with nitrogenous species, which tend to solvate easily [31]. In order to confirm these hypotheses, oxidation by-products were first identified by HPLC-DAD and then by GC–MS and LC-MS.

### 3.2.2. *Identification and characterization of by-products*

The chromatogram of plasma-treated paracetamol recorded as a function of exposure times 0 (i.e. control), 15 and 30 min displayed in Fig. 6 shows the appearance of by-products (280 nm), the majority more polar than the starting product, with shorter retention times than the starting product. The chromatograms also show an increase in by-product intensity as a function of treatment time.

The spectra of by-products ($S_1$ to $S_5$) identified from chromatograms (processed at 280 nm) of treated paracetamol are shown in Supplementary Data Fig. 6.

In order to cover almost all the oxidation by-products generated in the plasma phase, GC–MS analyses with and without derivatization to enable identification volatiles molecules, and LC-MS analyses were carried out. For LC-MS analyses, the dry residues of the plasma-treated solutions were solubilized in water (polar solvent) and acetonitrile (less polar) to explore virtually all by-products in terms of their polarities. Analyses were carried out on the sample with the highest degradation rate considering 30 min of plasma exposure, to minimize potential interference between intermediate by-products [32].

Fig. 7 and Fig. 8 show the GC–MS fragments obtained after derivatization and LC-MS fragments of the molecules identified by solubilizing dry extracts of the treated sample in acetonitrile (ACN) and water.

Regarding GC–MS fragments, the analyses carried out without derivatization do not enable us to identify any oxidation by-products. The latter are either very low-volatility (high molecular weight), which is in line with the peaks observed on the obtained chromatograms: highly polar species tend to have low volatility [33]. One solution is sylilation, i.e. grafting very specific functions onto molecules that are very difficult to volatilize: this technique is called Derivatization methods.

Derivatization of our samples enabled us to identify two by-products with molar masses above *m/z*: 151 (starting (paracetamol) molecule): *N*-(4-(4-hydroxyphenylamino) phenyl) acetamide (m/z: 242; B) and *N*-(4-aminophenyl) acetamide (m/z: 150; C), resulting respectively from recombination of the starting molecule (paracetamol) and its nitration. The identified by-products are not cited in the literature, enabling us to add them to the database of by-products resulting from the degradation of paracetamol (with concentration of 500 mg/L) by pulsed corona discharges.

In the case of LC-MS analysis, two compounds were identified: N-4-hydroxy-3-nitrophenyl) acetamide (m/z: 196) also known as 3-nitro-4-acetamidophenol and N-(3,4-dihydroxyphenyl) acetamide (m/z: 167) also known as Hydroxy-4-(*N*-acetyl)-aminophenol, in acetonitrile and water respectively (Fig. 8). Both intermediates (sub-product) compounds have been identified by high-resolution mass spectrometry (HRMS) and LC-MS/MS analysis in the literature as intermediates during the degradation of paracetamol by dielectric barrier discharge (DBD) treatment. However, the toxicity of the intermediates identified is not discussed by the authors [6,7].

The oxidation by-products identified by GC–MS and LC-MS analyses are mainly compounds derived from the nitration of paracetamol. This may be explained by the density of nitrogen species formed in the plasma phase using ambient air as background gas. Several authors underlined that the production of nitrogen species is favored in the pulsed spark regime [34]. This hypothesis in our case was confirmed by optical emission spectra given under the same plasma experimental conditions (see emission spectra given sub-section 3.1.3). About species, the applied high voltage to tip electrode generates a high inhomogeneous electric field near the incurved electrode. The action of this electric field gives first a sufficient high energy to electrons to start the processes of excitation, dissociation, and ionization of the main air molecules, in particular $N_2$ and $O_2$. Here is a representative selection of such primary electron impact reactions:

$$O_2 + e^- \rightarrow O_2^+ + 2e^- \quad (3)$$

$$O_2 + e^- \rightarrow 2O^{\cdot} + e^- \quad (4)$$

$$e^- + N_2 \rightarrow N_2^+ + 2e^- \quad (5)$$

$$N_2 + e^- \rightarrow 2\,N^{\cdot} + e^- \quad (6)$$

Positioning the ground electrode on the CDP reactor configuration presented in section 2.1 promotes acceleration of the streamer formed towards the surface of the liquid phase, creating thermo-electronic

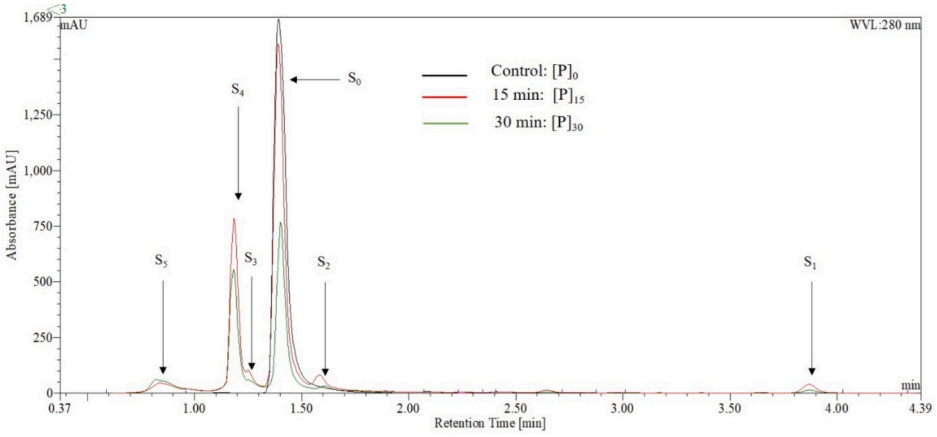


**Fig. 6.** Chromatogram (processed at 280 nm) obtained by HPLC-DAD of plasma-treated paracetamol recorded as a function of exposure time 0, 15 and 30 min (10 kV, 10 kHz, gap: 4 mm, 1 μs, 100 mL and 100 μm of tip radius).

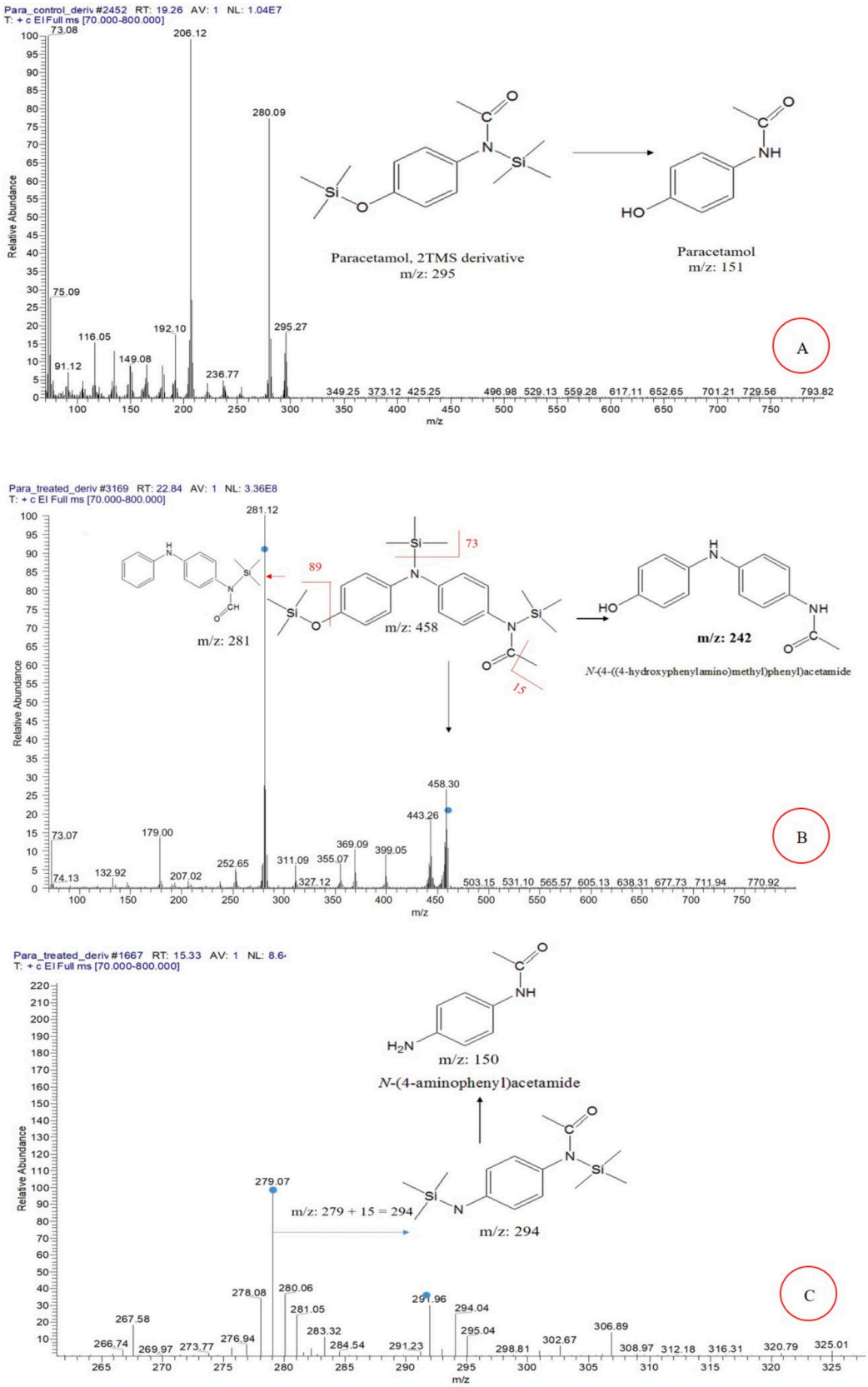


**Fig. 7. Up** (A) GC–MS fragments with derivatization of paracetamol. **Middle (B)** Fragments of the oxidation by-product 1 identified after derivatization. **Bottom** (C) Fragments of the oxidation by-product 2 identified after derivatization.

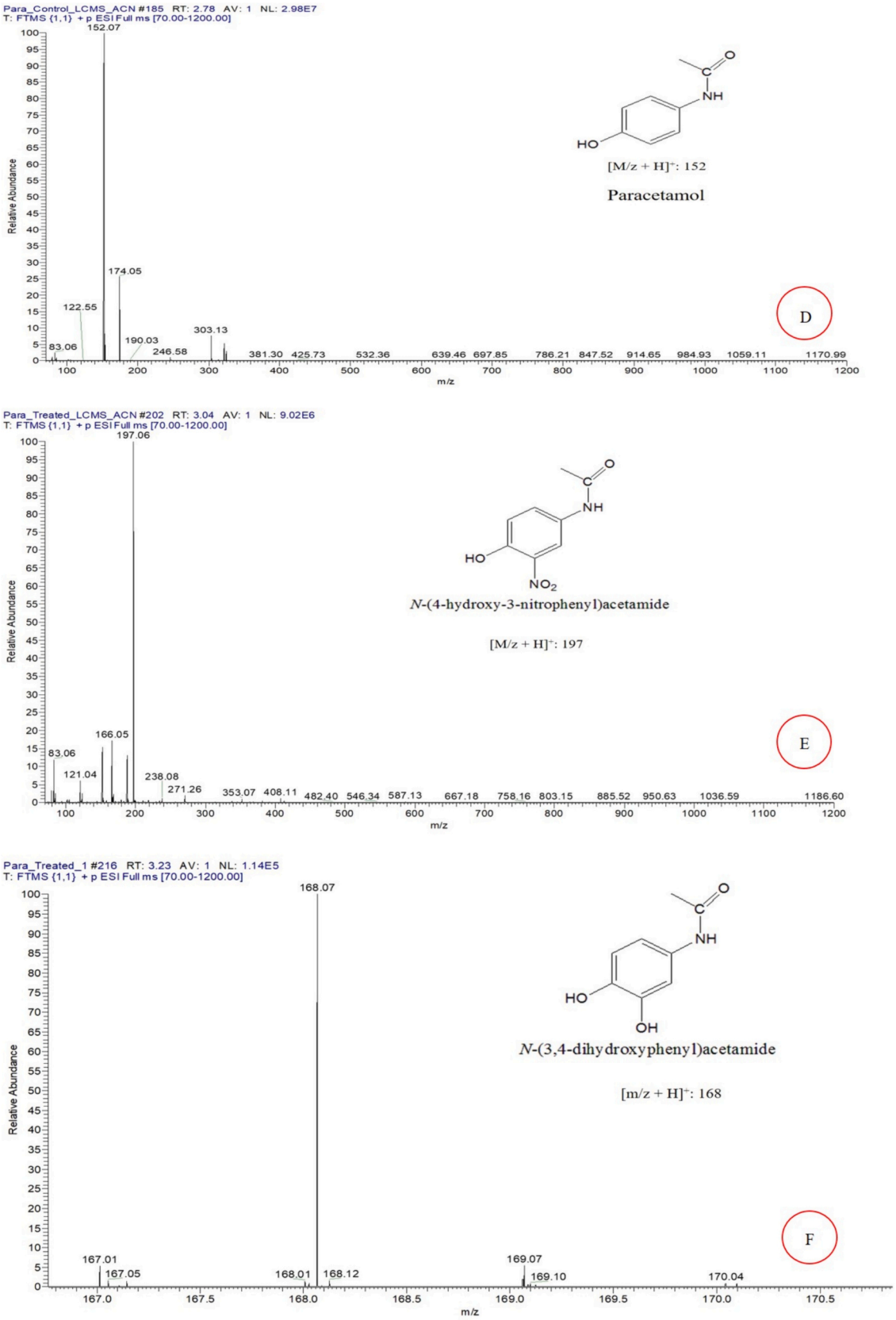


**Fig. 8. Up (D):** (Left) LC-MS fragments of paracetamol solubilized in acetonitrile (ACN) and Water. Middle **(E)**: LC-MS fragment of the oxidation by-product 3 identified in the dry extract solubilized ACN. **Bottom**(F): LC-MS fragments of the oxidation by-product 4 identified in the water-solubilized dry extract.

hydrodynamic convection at the interface and local water evaporation. The presence of water vapours in the gas phase (boundary layer close to the interface on the gas side) favors the production of new species by energetic electron impacts:

$$e^- + H_2O \rightarrow 2H + O + e^- \quad (7)$$

$$e^- + H_2O \rightarrow H^- + OH \quad (8)$$

These electron-molecule impacts generally occur inside the filamentary structure of corona discharge thus generating high concentrations of primary radicals (O, N, OH., etc.), metastable as $N_2(A^3\Sigma_u^+)$ and ions ($N^+$, $O^+$, $N_2^+$, $O_2^+$, $O^-$, etc.) in each discharge filament from the tip up to the water surface. These primary species in turn collide the surrounding air particularly in the gas-liquid interface to form stable secondary reactive species ($O_3$, $ONOO^-$, $H_2O_2$, $NO_3$, $NO_2$, etc.). The latter and energetic electrons interact with the liquid surface to form, following complex pathways, RONS of our interest.

There are many possible interaction mechanisms for the formation of the oxidation identified by-products. In an environment rich in nitrogenous species, such as spark discharge in air, and in the presence of

Mechanism sub-product **B**

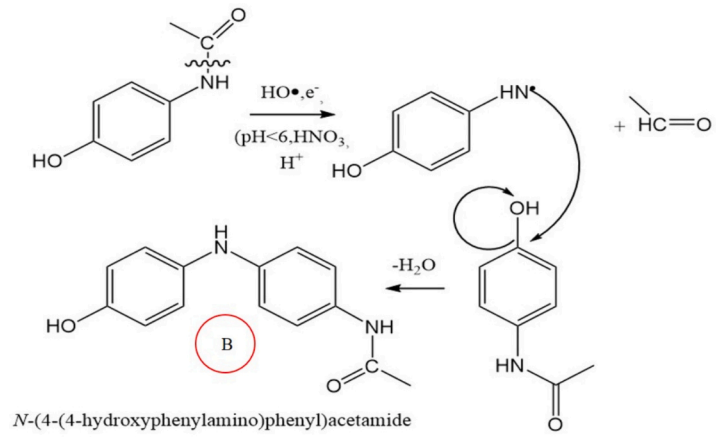


*N*-(4-(4-hydroxyphenylamino)phenyl)acetamide

Mechanism sub-product **C**

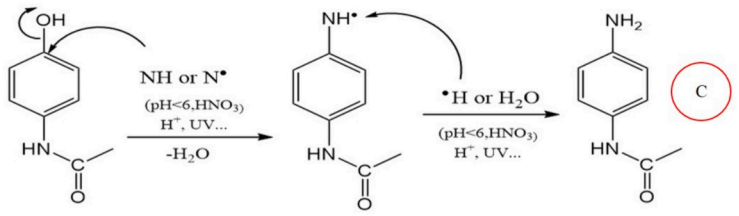


*N*-(4-aminophenyl)acetamide

Mechanism sub-product **E**

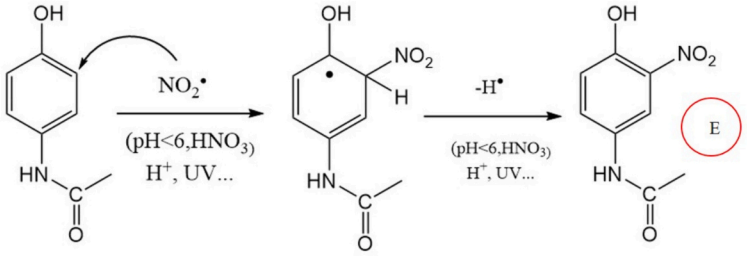


Mechanism sub-product **F**

*N*-(4-hydroxy-3-nitrophenyl)acetamide

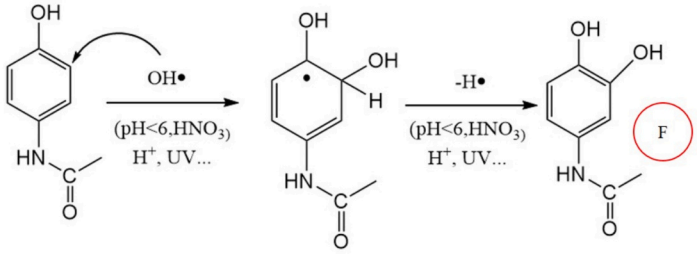


*N*-(3,4-dihydroxyphenyl)acetamide

**Fig. 9.** Probable by-product formation mechanism identified by GC–MS, and LC-MS analysis.

highly reactive sites on the starting molecule, such as double bonds [35], several types of reactions can take place.

### 3.2.3. Paracetamol degradation pathways in CDP

Fig. 9 shows the formation mechanisms of acetamide *N*-(4-(4-hydroxyphenylamino) phenyl) acetamide (*m/z*: 242) and *N*-(4-aminophenyl) acetamide (m/z: 150), *N*-4-hydroxy-3-nitrophenyl) acetamide (m/z: 196) and *N*-(3,4-dihydroxyphenyl) acetamide (m/z: 167).

For N-(4((hydroxyphenylamino)methyl) phenyl) acetamide (m/z: 242), the reaction mechanism involves two steps: the carboxyl group leaves a highly reactive vacant site on the intermediate 4-aminophenol anion or 4-aminophenol radical, which then reacts with another paracetamol molecule, releasing a molecule of water ($H_2O$). Mechanism subproduct C for the formation of N-(4-aminophenyl) acetamide (m/z: 150) is relatively straightforward, involving a single step of substitution of the OH group by -$NH_2$.

About by-products identified by LC-MS (N-4-hydroxy-3-nitrophenyl) acetamide (m/z: 196) and N-(3,4-dihydroxyphenyl) acetamide (m/z: 167), the pathways formations are classic [6,7]: in the first case, nitration by the $^{\cdot}NO_2$ radical for example, followed by substitution of the additional proton by the $OH^{\bullet}$ radical and other reactive species. The presence of $^{\cdot}NO_2$ radicals can be explained by two hypotheses i) the formation of radicals in the gas phase very close to the interface (boundary layer) which then diffuses into the liquid phase due to its solubility (Henry's law solubility constant $1.4*10^{-4}$ mol•$m^{-3}$•$Pa^{-1}$) compared to its counterpart $^{\cdot}NO$ (Henry's law solubility constant $1.9*10^{-5}$ mol•$m^{-3}$•$Pa^{-1}$). However, the concentration of $^{\cdot}NO$ in the gas phase is generally two orders of magnitude higher than the concentration of $\bullet NO_2$. ii) the presence of $^{\cdot}NO_2$ in the liquid phase can also be explained by the presence of reactive and unstable intermediate species such as peroxynitrite ($ONOO^-$). In an acidic environment such as ours (pH around 3), peroxonitrite and its conjugate acid (ONOOH) dissociate either to form the $^{\cdot}NO_2$ radical or nitric acid in solution according to the following reactions [36–39]:

$$ONOO_{(aq)} \rightarrow {}^{\bullet}NO_{2(aq)} + HO\bullet_{(aq)} \quad (9)$$

$$ONOO_{(aq)} \rightarrow HNO_{3(aq)} \quad (10)$$

When comparing the standard potential (supplementary data, Table 3) of the species produced by the plasma and potentially present in the liquid phase, we can see that the standard potential of the systems $ONOO^-/NO_2$ ($E^\circ = 2.44$ V/SHE) is very close to the reference systems, i.e. $OH^{\bullet}/H_2O$, which is $E^\circ = 2.85$ V/SHE [40]. The $ONO_2H/NO_2$ system has a lower potential than ozone but a higher potential than $NO_3^-/HNO_2$. Although ozone has a high standard potential ($E^\circ = 2.07$ V/SHE), its degradation under the effect of temperature would inhibit its contribution to the oxidation of paracetamol in our reactor (solution temperature is equal to 67 °C throughout the treatment), unlike nitrogenous species whose production is favored at high temperature. In the case of by-product F (Hydroxy-4-(*N*-acetyl)-aminophenol we observe an oxidation/substitution reaction by the radical oxidizing species at the preferential site. In our case (solution temperature is equal to 37 °C under acid pH) the probable oxidizing species are $OH^{\bullet}$, peroxynitrite ($ONOO^-$), $OH_2$… given their strongly oxidizing nature presented in the Supplementary Data Table 3.

The intermediate by-products of paracetamol oxidation identified in this work are for the most part nitrogenous products that could be used in green agriculture. However, the temperature variation observed in the CDP system for paracetamol degradation and the system's energy consumption are limiting factor for achieving the ultimate oxidation of paracetamol (500 mg/L) by the CDP system. Thus, for a potential large-scale application of CDP, the energy cost should be minimized by either: i) directing the formation of oxidation products towards biodegradable products (in our case, a biodegradability study of the by-products identified is necessary). In this case, the reactions must be initiated by the plasma and the degradation of the pharmaceutical pollutants by the microorganisms must be continued (plasma/microorganism coupling), ii) by integrating a cooling system and controlling the nature and flow rate of the gas to favor the production of reactive oxygen species.

However, the question that arises is the toxicity of the by-products obtained, which may be intermediates in the process of achieving complete oxidation of paracetamol.

### 3.2.4. In vitro cytotoxicity assessment

The toxicity of paracetamol and its degradation by-products was determined using the survival rate of HEK-293. The human embryonic kidney (HEK) 293 cell line has been widely distributed since its isolation >25 years ago [41]. This cell line is considered healthy, making it the preferred choice for demonstrating the toxicity of oxidation by-products.

Fig. 10 shows the viability percentage of cells exposed to a Tamoxifen solution (37 mg/L), i.e. the positive control, the untreated paracetamol solution and two solutions of plasma treated paracetamol during 15 min and 30 min respectively.

According to Fig. 10, the percentage of viability is not affected in the presence of plasma-treated paracetamol solutions tested at 50 mg/L: the percentage obtained for control and treated solutions remains unchanged at around 90 %. However, there is a decrease in viability of around 4 % (not significant) for the sample treated for 30 min compared with the untreated paracetamol solution. The percentage viability of the positive control tested at a concentration equal to 37 mg/L is 40 %, i.e. 60 % cell death. Compared with other pharmaceutical molecules that generate toxic by-products after plasma treatment [14–16], this study shows that the by-products identified following treatment of a high concentration (500 mg/L) of paracetamol with CDP are not toxic. The no generation of toxic by-products paracetamol oxidation using PCD system seems to be one of the legitimate solutions to the growing problem of water pollution by drugs and hospital effluents. Treated waste effluents can be recycled for agriculture and other respectful of the environment.

## 4. Conclusion

This study demonstrates the potential of the ambient air spark corona discharge generated by a tip-to-water configuration powered by a pulsed high voltage for the degradation of high-concentration pharmaceutical pollutants. It also highlights the non-toxicity of the resulting oxidation by-products, emphasizing the potential challenge of their subsequent removal. Therefore, gaseous and especially aqueous RONS produced by this corona spark discharge is very competitive for the degradation of this type of pollutant even when its concentration is relatively high. Indeed, we chosen the pharmaceutical pollutant (paracetamol) at a concentration of 500 mg/L to make the present study more complex than those of the literature, which used only 25 mg/L, i.e. 20 times less. For all the corona discharge parameters (tip-to-water distance, and voltage magnitude) selected in the present work, we obtained an optimal production of RONS leady to a very acceptable degradation

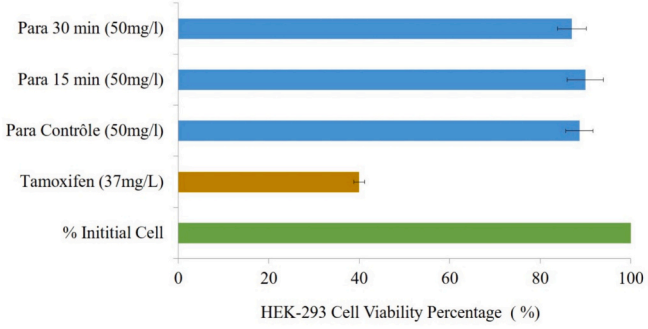


**Fig. 10.** Effect of plasma-treated solutions on the viability of healthy cells HEK-293 (10 kV, 10 kHz, gap: 4 mm,1 μs, 100 mL and 100 μm of tip radius).

rate of around 60 %, energy efficiency value (G50) equal to 0.52 g/kWh as a performance indicator.

Then, HPLC-DAD, GC–MS and LC-MS analyses enabled us to identify and characterize two new paracetamol oxidation by-products (not previously identified in the literature): *N*-(4-(4-hydroxyphenylamino) phenyl) acetamide (*m/z*: 242) and *N*-(4-aminophenyl) acetamide (m/z: 150). The majority of these new by-products are derived from the nitration of paracetamol since the considered corona spark regime generates energetic electrons able to dissociate not only oxygen molecules but also nitrogen one having a much higher energy dissociation. This could be explained by the wide variety of nitrogen species formed in the plasma phase, as shown by optical emission spectroscopy analysis.

The identified oxidation by-products revealed their non-toxicity on healthy cell lines, HEK-293, opening a field of application in for example in agriculture because nitro generated compounds are very beneficial for seed germination and plant growth. Last, our study provides useful guidelines for the development of an effective and sustainable treatment of wastewater containing pharmaceutical pollutants and can be envisaged as a solution for the treatment and recovery of hospital liquid effluents.

## CRediT authorship contribution statement

**Djakaou Iya-Sou:** Writing – original draft, Visualization, Validation, Supervision, Software, Methodology, Investigation, Formal analysis, Data curation, Conceptualization. **Nofel Merbahi:** Writing – original draft, Validation, Supervision, Resources, Project administration, Methodology, Funding acquisition, Formal analysis, Conceptualization. **Jalloul Bouajila:** Visualization, Validation, Supervision, Software, Project administration, Methodology, Investigation, Formal analysis, Data curation, Conceptualization. **Mohammed Yousfi:** Writing – original draft, Visualization, Validation, Supervision, Software, Resources, Methodology, Formal analysis, Data curation, Conceptualization.

## Declaration of competing interest

The authors declare that they have no known competing financial interests or personal relationships that could have appeared to influence the work reported in this paper.

## Data availability

Data will be made available on request.

## Appendix A. Supplementary data

Supplementary data to this article can be found online at https://doi.org/10.1016/j.jwpe.2024.106127.

## References


[1] E.S. Massima Mouele, J.O. Tijani, K.O. Badmus, O. Pereao, O. Babajide, C. Zhang, T. Shao, E. Sosnin, V. Tarasenko, O.O. Fatoba, Removal of pharmaceutical residues from water and wastewater using dielectric barrier discharge methods. A review, Int. J. Environ. Res. Public Health 18 (2021) 1683, https://doi.org/10.3390/ijerph18041683.

[2] A. Sokolova, M. Kråkströmb, P. Eklundb, L. Kronbergb, M. Louhi-Kultanena, Abatement of amoxicillin and doxycycline in binary and ternary aqueous solutions by gas-phase pulsed corona discharge oxidation, Chem. Eng. J. 334 (2018) 673–681, https://doi.org/10.1016/j.cej.2017.10.071.

[3] I. Beate, R. Baumgartner Escher, M. Koller, K. Treyer, J. Lienert, C. McArdell, Environmental toxicology and risk assessment of pharmaceuticals from hospital wastewater, Water Res. 45 (2011) 75–92, https://doi.org/10.1016/j.watres.2010.08.019.

[4] C. Puyang, J. Han, H. Guo, Degradation of emerging contaminants in water by a novel non-thermal plasma/periodate advanced oxidation process: performance and mechanisms, Chem. Eng. J. 483 (2024) 149194, https://doi.org/10.1016/j.cej.2024.149194.

[5] M. Parolini, Toxicity of the Non-Steroidal Anti-Inflammatory Drugs (NSAIDs) acetylsalicylic acid, paracetamol, diclofenac, ibuprofen and naproxen towards freshwater invertebrates: a review, Sci. Total Environ. 740 (2020) 140043, https://doi.org/10.1016/j.scitotenv.2020.140043.

[6] Y. Baloul, O. Aubrey, H. Rabat, C. Colas, B. Maunit, D. Hong, Paracetamol degradation in aqueous solution by non-thermal plasma, Eur. Phys. J. Appl. Phys. 79 (2017) 30802, https://doi.org/10.1051/epjap/2017160472.

[7] X.Y. Pan, X.C. Qiao, Influences of nitrite on paracetamol degradation in dielectric barrier discharge reactor, Ecotoxicol. Environ. Saf. 180 (2019) 610–616, https://doi.org/10.1016/j.ecoenv.2019.04.037.

[8] P. Bruggeman, et al., Plasma–liquid interactions: a review and roadmap, Plasma Sources Sci. Technol. 25 (2016) 053002, https://doi.org/10.1088/0963-0252/25/5/053002.

[9] N. Shahsavari, X. Zhang, Microbubble-enhanced cold plasma activation for water decontamination: degradation dynamics and energy yield in relation to pollutant concentration, total volume and flow rate of water, J. Water Process Eng. 55 (2023) 104169, https://doi.org/10.1016/j.jwpe.2023.104169.

[10] Y. He, J. Shen, N.S. Alharbi, et al., Volatile organic compounds degradation by non-thermal plasma: a review, Environ. Sci. Pollut. Res. (2023), https://doi.org/10.1007/s11356-023-25524-5.

[11] N. Korichi, O. Aubrey, H. Rabat, B. Cagnon, D. Hong, Paracetamol degradation by catalyst enhanced non-thermal plasma process for a drastic increase in the mineralization rate, Catalysts 10 (2020) 959, https://doi.org/10.3390/catal10090959.

[12] S. Slamani, F. Abdelmalek, M.R. Ghezzar, A. Addou, Initiation of Fenton process by plasma gliding arc discharge for the degradation of paracetamol in water, J. Photochem. Photobiol. A Chem. 359 (2018) 1–10, https://doi.org/10.1016/j.jphotochem.2018.03.032.

[13] G. Iervolino, V. Vaiano, V. Palma, Enhanced removal of water pollutants by dielectric barrier discharge non-thermal plasma reactor, Sep. Purif. Technol. 215 (2019) 155–162, https://doi.org/10.1016/j.seppur.2019.01.007.

[14] R.K. Singh, L. Philip, S. Ramanujam, Rapid degradation, mineralization and detoxification of pharmaceutically active compounds in aqueous solution during pulsed corona discharge treatment, Water Res. 121 (2017) 20–36, https://doi.org/10.1016/j.watres.2017.05.006.

[15] A. Aguera, L.A. Perez Estrada, I. Ferrer, E.M. Thurman, S. Malato, A.R. Fernandez-Alba, Application of time-of-flight mass spectrometry to the analysis of phototransformation products of diclofenac in water under natural sunlight, J. Mass Spectrom.: JMS 40 (2005) 908–915, https://doi.org/10.1002/jms.867.

[16] J. Madhavan, F. Grieser, M. Ashokkumar, Combined advanced oxidation processes for the synergistic degradation of ibuprofen in aqueous environments, J. Hazard. Mater. 178 (2010) 202–208, https://doi.org/10.1016/j.jhazmat.2010.01.064.

[17] A. Mraihi, N. Merbahi, M. Yousfi, A. Abahazem, O. Eichwald, Electrical and spectroscopic analysis of mono- and multi-tip pulsed corona discharges in air at atmospheric pressure, Plasma Sources Sci. Technol. 20 (2011) 065002 (12pp).

[18] N. Merbahi, M. Yousfi, J.P. Gardou, Electric and spectroscopic analysis of surface corona discharges in ambient air and comparison with volume corona discharges, IEEE Transsactions on Plasma Science 40 (4) (2012), https://doi.org/10.1109/TPS.2012.2184804.

[19] S. Idoudi, K.B. Othman, J. Bouajila, A. Tourrette, M. Romdhane, W. Elfalleh, Influence of extraction techniques and solvents on the antioxidant and biological potential of different parts of Scorzonera undulata, Life 13 (2023) 904, 10.3390/.

[20] T. Ben Khadher, S. Aydi, M. Mars, J. Bouajila, Study on the chemical composition and the biological activities of Vitis vinifera stem extracts, Molecules 27 (2022) 3109, https://doi.org/10.3390/molecules27103109.

[21] B.R. Locke, M. Sato, P. Sunka, M.R. Hoffmann, J.S. Chang, Electrohydraulic discharge and nonthermal plasma for water treatment, Ind. Eng. Chem. Res. 45 (2006) 882–905, https://doi.org/10.1021/ie050981u.

[22] C. Bradu, K. Kutasi, M. Magureanu, N. Puac, S. Živkovic, Reactive nitrogen species in plasma-activated water: generation, chemistry and application in agriculture, J. Phys. D. Appl. Phys. 53 (2020) 223001, https://doi.org/10.1088/1361-6463/ab795a.

[23] Z. Liu, C. Zhou, D. Liu, T. He, L. Guo, D. Xu, M.G. Kong, Quantifying the concentration and penetration depth of long-lived RONS in plasma-activated water by UV absorption spectroscopy, AIP Adv. 9 (2019) 015014, https://doi.org/10.1063/1.5037660.

[24] A.H. Zerrouki, Y. Motomura, M. Ikeda, M. Yousfi Jinno, Optical emission spectroscopy characterizations of micro-air plasma used for simulation of cell membrane, Plasma Phys. Control. Fusion 58 (2016) 075006, https://doi.org/10.1088/0741-3335/58/7/075006.

[25] M.D. Calzada, M. Saez, M.C. Garcia, Characterization and study of the thermodynamic equilibrium departure of an argon plasma flame produced by a surface-wave sustained discharge, J. Appl. Phys. 88 (2000) 34–39, https://doi.org/10.1063/1.373619.

[26] M. Gromov, K. Leonova, N. De Geyter, R. Rino Morent, R. Snyders, N. Britun, A. Nikiforov, $N_2$ oxidation kinetics in a ns-pulsed discharge above a liquid electrode, Plasma Sources Sci. Technol. 1 (30) (2021) 065024, https://doi.org/10.1088/1361-6595/abff71.

[27] S. Kooshki, P. Pareek, M. Janda, Z. Machala, Selective reactive oxygen and nitrogen species production in plasma-activated water via dielectric barrier discharge reactor: an innovative method for tuning and its impact on dye degradation, J. Water Process Eng. 63 (2024) 105477, https://doi.org/10.1016/j.jwpe.2024.105477.

[28] M. Loeb, B. Leonard, J.M. Meek, The mechanism of spark discharge in air at atmospheric pressure, J. Appl. Phys. 11 (2004) 438–447, https://doi.org/10.1063/1.1712792.

[29] M. Bajaj, C. Gallert, J. Winter, Biodegradation of high phenol containing synthetic wastewater by an aerobic fixed bed reactor, Bioresour. Technol. 99 (2008) 8376–8381, https://doi.org/10.1016/j.biortech.2008.02.057.
[30] P. Manoj, T. Charuvila Rayaroth, S. Aravindakumar, N.S. Noor, G. Boczkaj Shah, Advanced Oxidation Processes (AOPs) based wastewater treatment-unexpected nitration side reactions a serious environmental issue: a review, Chem. Eng. J. 430 (2022) 133002, https://doi.org/10.1016/j.cej.2021.133002.
[31] D. Iya-Sou, R.M. Ghezzar, M.E. Zekri, F. Abdelmalek, S. Cavadias, S. Ognier, Removal of model pollutants in aqueous solution by gliding arc discharge. Part II: modeling and simulation study, Plasma Chem. Plasma Process. 35 (2015) 143–157, https://doi.org/10.1007/s11090-014-9588-3.
[32] K.H. Hama Aziz, H. Miessner, A. Mahyar, S. Mueller, D. Kalass, D. Moeller, K. M. Omer, Removal of dichloroacetic acid from aqueous solution using non-thermal plasma generated by dielectric barrier discharge and nano-pulse corona discharge, Sep. Purif. Technol. 216 (2019) 51–57, https://doi.org/10.1016/j.seppur.2019.01.074.
[33] L. Yang, S.H. Budisulistiorini, G. Chen, X. Wang, M. Kuwata, The relationship between molecular size and polarity of atmospheric organic aerosol in Singapore and its implications for volatility and light absorption properties, ACS Earth Space Chem. 5 (2021) 3182–3196, https://doi.org/10.1021/acsearthspacechem.1c00274.
[34] P. Lu, D. Boehm, P. Bourke, P.J. Cullen, Achieving reactive species specificity within plasma-activated water through selective generation using air spark and glow discharges, Plasma Process. Polym. 14 (2017), https://doi.org/10.1002/ppap.201600207.
[35] E. Pretsch, P. Buhlmann, M. Badertscher, Structure Determination of Organic Compounds, ISBN 978-3-540-93809-5, 2000, https://doi.org/10.1007/978-3-540-93810-1.
[36] P. Pareek, S. Kooshki, P. Toth, M. Janda, Tuning composition of plasma activated water generated by transient spark discharge with electrospray, Chem. Eng. J. 493 (2024) 152583, https://doi.org/10.1016/j.cej.2024.152583.
[37] Y. Ye, Z. Zhou, S. Wang, Z. Fang, Characteristics and stability of pulsed gas–liquid discharge with the addition of photocatalysts, Plasma Chem. Plasma Process. 44 (2024) 335–352, https://doi.org/10.1007/s11090-023-10426-8.
[38] G. Bruno, S. Wenske, J.W. Lackmann, M. Lalk, T.V. Woedtke, K. Wende, On the liquid chemistry of the reactive nitrogen species peroxynitrite and nitrogen dioxide generated by physical plasmas, Biomolecules 10 (2020) 1687, https://doi.org/10.3390/biom10121687.
[39] C. Bradu, K. Kutasi, M. Magureanu, N. Puač, S. Živković, Reactive nitrogen species in plasma-activated water: generation, chemistry and application in agriculture, J. Phys. D. Appl. Phys. (2020), https://doi.org/10.1088/1361-6463/ab795a.
[40] J.L. Brisset, E. Hnatiuc, Peroxynitrite: a re-examination of the chemical properties of non-thermal discharges burning in air over aqueous solutions, Plasma Chem. Plasma Process. 32 (2012) 655–674, https://doi.org/10.1007/s11090-012-9384-x.
[41] G. Shaw, S. Morse, M. Ararat, F.L. Graham, Preferential transformation of human neuronal cells by human adenoviruses and the origin of HEK 293 cells, FASEB J. (2002), https://doi.org/10.1096/fj.01-0995fje.